2020

Deep UV Fluorescence Scanning Microscopy for Breast Tumor Margin Detection

Tongtong Lu
Marquette University

Julie M. Jorns
Medical College of Wisconsin

Mollie Patton
Medical College of Wisconsin

Renee Fisher
Marquette University

Amanda Emmrich
Medical College of Wisconsin

See next page for additional authors

Proceedings of SPIE 11229 : Advanced Biomedical and Clinical Diagnostics and Surgical Guidance Systems XVIII, Vol. 11229, (2020). DOI.

Deep UV Fluorescence Scanning Microscopy for Breast Tumor Margin Detection

Tongtong Lu
Marquette University (United States) and Medical College of Wisconsin (United States)

Julie Jorns
Medical College of Wisconsin (United States)

Mollie Patton
Medical College of Wisconsin (United States)

Renee Fisher
Marquette University (United States) and Medical College of Wisconsin (United States)

Amanda Emmrich
Medical College of Wisconsin (United States)

Todd Doehring
Abemis LLC (United States)

Taly Gilat-Schmidt
Marquette University (United States) and Medical College of Wisconsin (United States)

Dong Hye Ye
Marquette University (United States)

Tina Yen
Medical College of Wisconsin (United States)

Bing Yu
Marquette University (United States) and Medical College of Wisconsin (United States)

Abstract

Breast cancer is the most commonly diagnosed cancer among women. Positive margin status after breast-conserving surgery (BCS) is a predictor of higher rates of local recurrence. Intraoperative margin detection helps to complete tumor excision at the first operation. A margin tool that is capable of imaging all six margins of large lumpectomy specimens with both high resolution and fast speed (within 20 min) is yet to be developed. Deep UV light allows simultaneous excitation of multiple fluorophores and generating surface fluorescence images. We have developed a deep UV fluorescence scanning microscope (DUV-FSM) for slide-free, high-resolution and rapid examination of tumor specimens during BCS. The DUV-FSM uses a deep UV LED for oblique back illumination of freshly excised breast tissues stained with propidium iodide and Eosin Y and motorized XY stages for mosaic scanning. Fluorescence images are captured by a color CCD camera. Both invasive lobular carcinoma (ILC) and invasive ductal carcinoma (IDC) images showed excellent contrast from that of the normal cells in color, tissue texture, and cell density and shapes. This contrast have been consistently observed in all samples (n = 20) we have imaged so far. Statistical analysis showed a significant difference ($p<0.0001$) in nucleus-to-cytoplasm (NC) ratio between normal and invasive tissues. Thus, it may be utilized either visually by a trained individual or quantitatively by an algorithm to detect positive margins of lumpectomy specimens intraoperatively.

1. INTRODUCTION

Breast cancer is the most common cancer among women. In 2019, it is estimated that there will be over 268.000 women with newly diagnosed breast cancer in the United States,[1] of whom about a half to two-thirds will undergo BCS.[2-5] A positive margin is defined as cancer cells at the surface of the specimen. Women with positive margins have at least 2-fold increased risk of tumor recurrence in the same breast.[6, 7] Thus, women with positive margins are recommended to undergo further surgeries to achieve negative margins. Achieving negative margins during the first surgery results in lowered cost, better cosmesis and avoids additional emotional stress. Methods including 2D mammography,[8] digital tomosynthesis,[9] frozen section,[10] and cytologic imprint prep,[11] etc. have been investigated in breast margin detection during BCS. Optical methods including diffuse reflectance spectroscopy (DRS),[12] optical coherence tomography (OCT),[13] Raman spectroscopy,[14] photoacoustic tomography (PAT),[15] structured illumination imaging,[16] etc. have also been studied for margin assessment on ex vivo lumpectomy tissues. However, none of these methods has demonstrated the capability of inspecting 6 margins of an entire lumpectomy specimen with high microscopic resolution within a short period of time that is feasible to be implemented in the operation room. Microscopy with ultraviolet surface excitation (MUSE)[17] uses deep UV lights that penetrate very shallow in tissues for fluorescence excitation, which allows imaging superficial layers of the specimen in high resolution without other

complicated optical sectioning techniques. Previous studies using MUSE for breast tumor margin detection[18, 19] focus on generating H&E mimicking images by color mapping for histopathological assessment. We emphasize the importance of providing valuable margin status information directly to the surgeon within minutes in the operation room to guide surgeries.

2. METHODS

2.1 Imaging system

The experimental setup is shown in Figure 1. A 285 nm wavelength deep UV LED (M285L4, Thorlabs) is installed on the right side of a commercial inverted fluorescence microscope as oblique illumination for fluorescence excitation. The LED and the microscope are fastened on an optical breadboard to avoid possible relative position displacements. The excitation/emission filter block of the microscope is set to an empty position so that emission signals can directly follow the light path to the camera without filtering. Images are taken by a USB 3.0 color charge-coupled device (CCD) camera. The color camera is capable of capturing the fluorescence signals at different wavelengths simultaneously with no need to switch between emission filters. There is a tradeoff between imaging resolution and speed. Because time is precious in the operating room, a fast speed is highly desired and preferred in this application. A 4x apochromatic long working distance objective lens (Plan Fluor 4x, NA = 0.13) was selected to yield a large field-of-view (FOV) and hence accelerate the imaging speed. Large area scanning is achieved by an x-y motorized stage. The system is placed inside an optical dark enclosure to minimize influences from the environment and prevent UV leakage to personnel.

Figure 1.

Experimental setup. A deep UV LED is installed on the right side of a commercial inverted fluorescence microscope. The system is placed inside an optical dark enclosure for safety concerns and to avoid environmental lights.

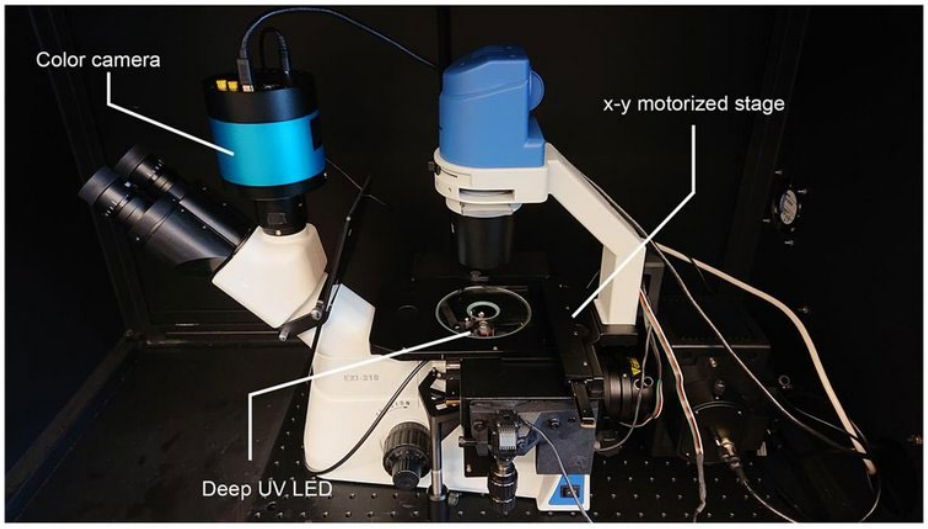

2.2 Specimen preparation

Human breast specimens were taken from lumpectomy and mastectomy cases by the Medical College of Wisconsin (MCW) Tissue Bank. All specimens included in this study were de-identified, therefore Institutional Review Board (IRB) and Institutional Biosafety Committee (IBC) reviews were exempted. The specimens were stained with 100 μg/ml propidium iodide (PI) for 20 seconds and 1.0 mg/ml eosin Y (EY) for 60 seconds. After that, the specimens were immersed into phosphate-buffered saline (PBS) solution to rinse away extra dyes on the specimen surface. PI stains cell nuclei and mainly exhibits red fluorescence when excited by deep UV lights.

EY stains cell cytoplasm and other tissue structures. EY mainly exhibits green fluorescence when excited. Because of the large wavelength gap (approximately 75 nm) between the fluorescence emission peaks of the two dyes, high contrast is expected between cell nuclei and other tissue structures. Stained specimens were placed on a quartz plate and pushed softly against the plate to get rid of air bubbles/liquid cavities, which can cause artifacts within images. Quartz is selected because it's UV-transparent and has low autofluorescence characteristics. The liquid on specimen surroundings was absorbed by Kimwipes.

2.3 Data processing

Individual scanning images were stitched together to create a whole specimen image for next step processing. A Fiji plugin named BaSiC was used for background and shading correction[20] caused by uneven illumination. Optimized collimation and alignment with multiple deep UV LEDs may reduce the effect of illumination unevenness in future studies. Image stitching was operated within Fiji.[21]

After imaging, specimens were transported back to MCW Tissue Bank for routine histology processing after imaging. Visual comparison of fluorescence images with the gold standard H&E images was performed by an experienced breast pathologist (Dr. Julie Jorns).

Uncontrolled division and growth of cancer cells cause multiple morphological changes in tumor regions. It is shown that cancer regions exhibit differences in cell density and nucleus-cytoplasm ratio (NC ratio) compared to normal regions.[22, 23] Moreover, NC ratios have already been used in cancer detection.[24-28] An algorithm based on edge detection and adaptive thresholding was applied for cell nuclei segmentation. Segmented specimen images were divided into 2 x 2 mm size patches. NC ratios were calculated for each small patch. Each patch was labeled as non-adipose normal (normal breast epithelium), adipose, ILC, and IDC in correlation with H&E images. Patches from ambiguous areas were discarded. For statistical analysis, the Generalized Estimating Equations (GEE) model was used to account for repeated observations per sample and the TUKEY adjustment was used for multiple pairwise comparisons.

3. RESULTS

3.1 Visual inspection

Figure 2 shows the fluorescence and H&E images of typical breast specimen structures. Adipose tissue appear as single or clustered rounded small droplets in dark green color and sparse pink nuclei as is shown in (a). H&E image from the same location has verified this in (f). Fluorescence image of benign lobules surrounded by fibrous stroma is shown in (b) and the corresponding H&E image in (g). Fibrous stroma has low nuclear density and hence appear mostly green in the fluorescence image. Benign lobules have higher nuclear density and nuclei are clustered in regular, rounded structures. This feature is more evident in the H&E image as terminal duct lobular units (TDLU). Benign ducts have two layers of epithelial cells and show a dense nuclei outlined duct in (c). The duct has an optically clear lumen in (h). However, it appears as a dark hole in the fluorescence image (c). Invasive tumors ILC and IDC are shown in (d) and (e) with their H&E images in (i) and (j), respectively. Tumor areas have a higher number of cell nuclei and appear in pink-red color. Infiltrating single-cell or Indian file pattern is visible in fluorescence image (d) for ILC.

Figure 2.

Fluorescence and H&E images of typical breast specimen structures. Normal tissues including predominantly adipose (with some normal glands at the lower right), benign lobules, and benign ducts with their H&E images are shown in (a), (b), (c) and (f), (g), (h), respectively. Invasive tumors including ILC and IDC with their H&E images are shown in (d), (e) and (i), (j), respectively.

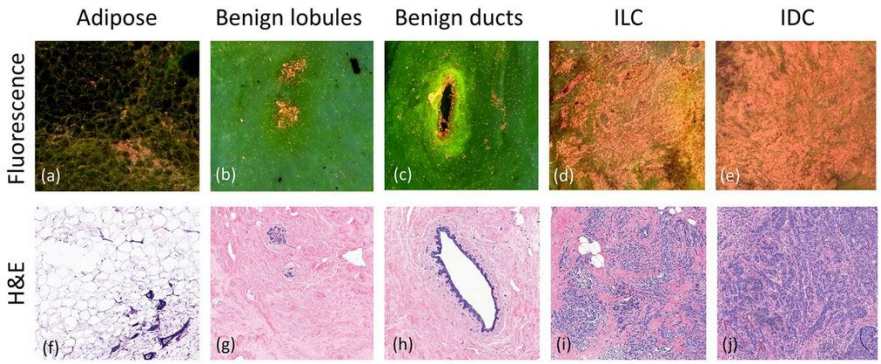

Figure 3 shows the image of a typical normal breast tissue. The gross specimen image is shown in (c). The sample size is approximately 19 x 14 mm. Stroma appears green in the fluorescence image (a) and pink in the H&E image (b). Scattered ducts and lobules are clearly visible in the fluorescence image.

Figure 3.

Typical normal breast tissue. (a) fluorescence image; (b) H&E image; (c) gross specimen image.

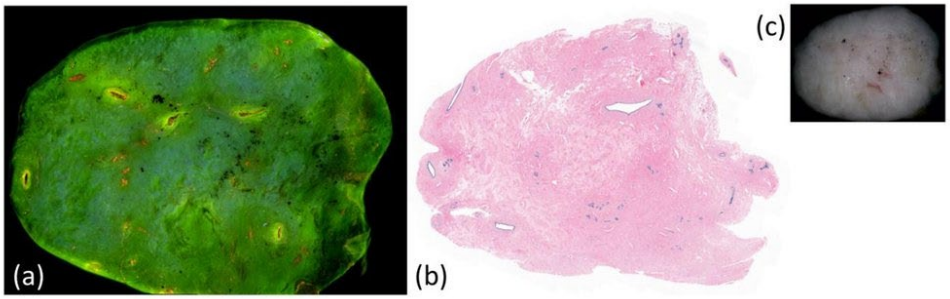

Figure 4 shows the image of a mixed IDC tissue. The specimen is acquired from a grade 3, ER/PR+, HER2- case. The gross specimen image is shown in (b). The specimen size is approximately 25 x 22 mm. Tumor regions on the left have high nuclear density and are easily distinguished visually from both the fluorescence image (a) and the H&E image (b).

Figure 4.

IDC tissue from case: grade 3, ER/PR+, HER2-. (a) fluorescence image; (b) gross specimen image; (c) H&E image.

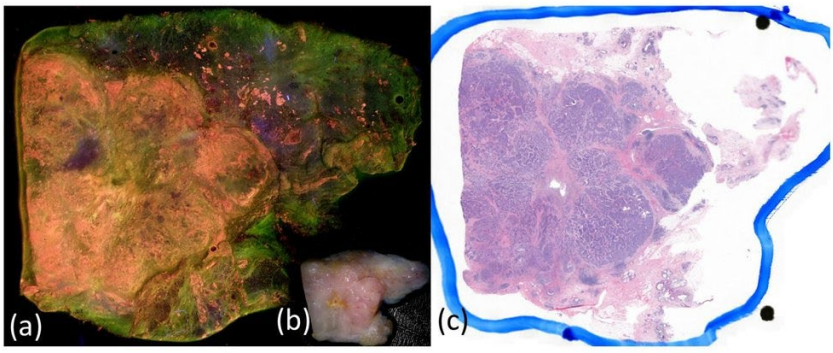

3.2 Statistical analysis

Results of statistical analysis on NC ratios are plotted in Figure 5. A total of 712 patches from the 20 breast tissue samples were obtained: 331 from 5 normal specimens, 189 from 3 adipose specimens, 26 from 3 ILC specimens

and 166 from 9 IDC specimens. Figure 5(a) is the boxplot of 4-class comparisons. There were significant differences between adipose and IDC, adipose and ILC, non-adipose normal and IDC, and non-adipose normal and ILC ($p<0.0001$). There was no significant difference between IDC and ILC ($p>0.5$), and adipose and non-adipose tissues ($p>0.1$). Figure 5(b) shows the boxplot of 2-class comparison. The invasive class includes IDC and ILC. The normal class includes adipose and non-adipose tissues. The GEE model indicates the estimate NC ratio of invasive tumor tissues is 0.19 higher than that of normal tissues with an empirical standard error of 0.03. A significant difference was observed between invasive tumor and normal tissues ($p<0.0001$).

Figure 5.

Statistical analysis on NC ratios results. Outliners were plot as red crosses. (a) 4-class comparisons. Significant differences are observed between IDC and adipose, IDC and non-adipose normal, ILC and adipose, and ILC and nonadipose normal. (b) 2-class comparison. A significant difference is observed between invasive tumor and normal tissues.

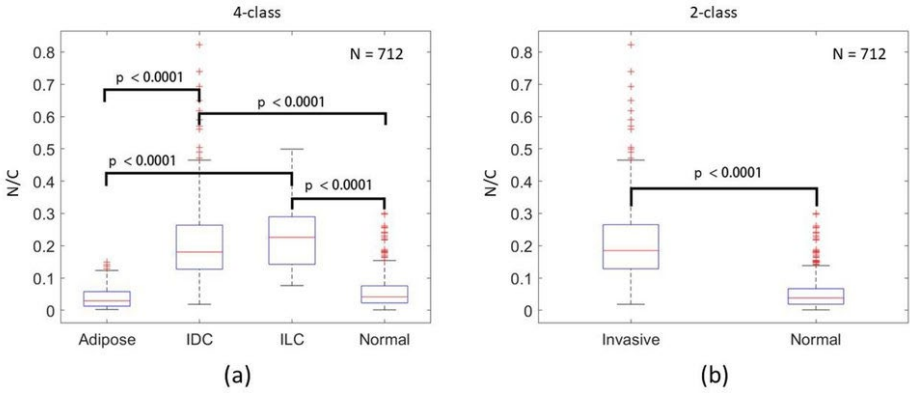

Table 1.

Summary of specimens and image patches generated.

Tissue type	Number of specimens	Number of patches
Adipose	3	189
Non-adipose normal	5	331
IDC	9	166
ILC	3	26
Total	20	712

4. DISCUSSIONS AND CONCLUSION

Visual inspection shows a good correlation between fluorescence and H&E images. Invasive tumor exhibits differences in color, tissue texture, cell density and shapes compared to normal tissues. Common human breast tissue structures are easily identifiable in fluorescence images. Of note it might be difficult to co-register all features between fluorescence and H&E images. There are mainly two reasons. First, specimen shape can change between imaging and the formalin-fixed paraffin-embedded (FFPE) histology process; Second, there is an average ~200 µm cut depth into the embedded tissue block in order to get a full face section of the tissue for H&E slide preparation. Fluorescence images only capture the top dozens of µm from the specimen surface. In addition, same tissue structure can appear differently in fluorescence and H&E images, such as benign ducts having optical clearly lumina in H&E images while this is not the case in fluorescence images. There are just differences between the two techniques but that the correlates are consistent and easily translatable between methods. Statistical analysis on NC ratios shows a significant difference between invasive tumors and normal

tissues, which implies that NC ratio may be used to develop an algorithm to detect invasive tumor regions automatically. However, in this study, the patch size is 2 x 2 mm. The spatial resolution cannot reach below 2 mm, which means small size tumor regions might not be detected by this method. Future studies will explore using more features in differentiating tumor regions from normal tissue.

In conclusion, a commercial inverted fluorescence microscope has been converted to a DUV-FSM with preliminary deep UV fluorescence images showing values as a promising intraoperative tool for rapid imaging of tumor margins during BCS. Distinct visual contrasts are identified between invasive tumor and normal regions. Statistically significant differences in NC ratio also distinguish tumor and normal tissue. Future work will focus on optimizing the imaging system, collecting more specimen data, and exploring other methods for tumor/normal classification.

5. ACKNOWLEDGEMENTS

This study has been supported by the Marquette University College of Engineering GHR Foundation grant (Dr. Bing Yu and Dr. Taly Gilat-Schmidt), Marquette University startup grant (Dr. Bing Yu), and We Care Fund, Medical College of Wisconsin, Department of Surgery (Dr. Tina Yen and Dr. Bing Yu).

REFERENCES

[1] R. L. Siegel, K. D. Miller, and A. Jemal, "Cancer statistics, 2019," CA Cancer J Clin, 69 (1), 7 –34 (2019). https://doi.org/10.3322/caac.v69.1

[2] R. Nash, M. Goodman, C. C. Lin et al., "State Variation in the Receipt of a Contralateral Prophylactic Mastectomy Among Women Who Received a Diagnosis of Invasive Unilateral Early-Stage Breast Cancer in the United States, 2004-2012," JAMA Surg, 152 (7), 648 –657 (2017). https://doi.org/10.1001/jamasurg.2017.0115

[3] S. M. Wong, R. A. Freedman, Y. Sagara et al., "Growing Use of Contralateral Prophylactic Mastectomy Despite no Improvement in Long-term Survival for Invasive Breast Cancer," Ann Surg, 265 (3), 581 –589 (2017). https://doi.org/10.1097/SLA.0000000000001698

[4] K. L. Kummerow, L. Du, D. F. Penson et al., "Nationwide trends in mastectomy for early-stage breast cancer," JAMA Surg, 150 (1), 9 –16 (2015). https://doi.org/10.1001/jamasurg.2014.2895

[5] O. Kantor, C. Pesce, K. Kopkash et al., "Impact of the Society of Surgical Oncology-American Society for Radiation Oncology Margin Guidelines on Breast-Conserving Surgery and Mastectomy Trends," J Am Coll Surg, (2019). https://doi.org/10.1016/j.jamcollsurg.2019.02.051

[6] M. L. Marinovich, L. Azizi, P. Macaskill et al., "The Association of Surgical Margins and Local Recurrence in Women with Ductal Carcinoma In Situ Treated with Breast-Conserving Therapy: A Meta-Analysis," Ann Surg Oncol, 23 (12), 3811 –3821 (2016). https://doi.org/10.1245/s10434-016-5446-2

[7] N. Houssami, P. Macaskill, M. L. Marinovich et al., "The association of surgical margins and local recurrence in women with early-stage invasive breast cancer treated with breast-conserving therapy: a meta-analysis," Ann Surg Oncol, 21 (3), 717 –30 (2014). https://doi.org/10.1245/s10434-014-3480-5

[8] R. A. Graham, M. J. Homer, C. J. Sigler et al., "The efficacy of specimen radiography in evaluating the surgical margins of impalpable breast carcinoma," AJR Am J Roentgenol, 162 (1), 33 –6 (1994). https://doi.org/10.2214/ajr.162.1.8273685

[9] K. U. Park, H. M. Kuerer, G. M. Rauch et al., "Digital Breast Tomosynthesis for Intraoperative Margin Assessment during Breast-Conserving Surgery," Ann Surg Oncol, 26 (6), 1720 –1728 (2019). https://doi.org/10.1245/s10434-019-07226-w

[10] T. P. Olson, J. Harter, A. Munoz et al., "Frozen section analysis for intraoperative margin assessment during breast-conserving surgery results in low rates of re-excision and local recurrence," Ann Surg Oncol, 14 (10), 2953 –60 (2007). https://doi.org/10.1245/s10434-007-9437-1

[11] J. J. Keating, C. Fisher, R. Batiste et al., "Advances in intraoperative margin assessment for breast cancer," Cuur Surg Rep, 4 (2016).

[12] J. Q. Brown, T. M. Bydlon, L. M. Richards et al., "Optical Assessment of Tumor Resection Margins in the Breast," IEEE Journal of Selected Topics on Quantum Electronics, 16 530 –544 (2010). https://doi.org/10.1109/JSTQE.2009.2033257

[13] F. T. Nguyen, A. M. Zysk, E. J. Chaney et al., "Intraoperative evaluation of breast tumor margins with optical coherence tomography," Cancer Res, 69 (22), 8790 –6 (2009). https://doi.org/10.1158/0008-5472.CAN-08-4340

[14] A. S. Haka, Z. Volynskaya, J. A. Gardecki et al., "Diagnosing breast cancer using Raman spectroscopy: prospective analysis," J Biomed Opt, 14 (5), 054023 (2009). https://doi.org/10.1117/1.3247154

[15] R. Li, P. Wang, L. Lan et al., "Assessing breast tumor margin by multispectral photoacoustic tomography," Biomed Opt Express, 6 (4), 1273 –81 (2015). https://doi.org/10.1364/BOE.6.001273

[16] A. Mazhar, S. Dell, D. J. Cuccia et al., "Wavelength optimization for rapid chromophore mapping using spatial frequency domain imaging," J Biomed Opt, 15 (6), (2010). https://doi.org/10.1117/1.3523373

[17] F. Fereidouni, Z. T. Harmany, M. Tian et al., "Microscopy with ultraviolet surface excitation for rapid slide-free histology," Nature Biomedical Engineering, 1 (12), 957 –966 (2017). https://doi.org/10.1038/s41551-017-0165-y

[18] W. Xie, Y. Chen, Y. Wang et al., "Microscopy with ultraviolet surface excitation for wide-area pathology of breast surgical margins," J Biomed Opt, 24 (2), 1 –11 (2019). https://doi.org/10.1117/1.JBO.24.2.026501

[19] T. Yoshitake, M. G. Giacomelli, L. M. Quintana et al., "Rapid histopathological imaging of skin and breast cancer surgical specimens using immersion microscopy with ultraviolet surface excitation," Sci Rep, 8 (1), 4476 (2018). https://doi.org/10.1038/s41598-018-22264-2

[20] T. Peng, K. Thorn, T. Schroeder et al., "A BaSiC tool for background and shading correction of optical microscopy images," Nat Commun, 8 14836 (2017). https://doi.org/10.1038/ncomms14836

[21] S. Preibisch, S. Saalfeld, and P. Tomancak, "Globally optimal stitching of tiled 3D microscopic image acquisitions," Bioinformatics, 25 (11), 1463 –5 (2009). https://doi.org/10.1093/bioinformatics/btp184

[22] R. S. Saad, and J. F. Silverman, "CHAPTER 25 - Breast] W.B. Saunders, Edinburgh," (2008).

[23] M. N. Gurcan, A. Madabhushi, H. M. Reynolds et al., "Cell density in prostate histopathology images as a measure of tumor distribution," International Society for Optics and Photonics, (2014).

[24] Y. Tang, J. Carns, and R. R. Richards-Kortum, "Line-scanning confocal microendoscope for nuclear morphometry imaging," J Biomed Opt, 22 (11), 1 –6 (2017). https://doi.org/10.1117/1.JBO.22.11.116005

[25] D. Shin, M. H. Lee, A. D. Polydorides et al., “Quantitative analysis of high-resolution microendoscopic images for diagnosis of neoplasia in patients with Barrett’s esophagus,” Gastrointest Endosc, 83 (1), 107 –14 (2016). https://doi.org/10.1016/j.gie.2015.06.045

[26] B. D. Grant, J. H. Fregnani, J. C. Possati Resende et al., “High-resolution microendoscopy: a point-of-care diagnostic for cervical dysplasia in low-resource settings,” Eur J Cancer Prev, 26 (1), 63 –70 (2017). https://doi.org/10.1097/CEJ.0000000000000219

[27] T. Quang, R. A. Schwarz, S. M. Dawsey et al., “A tablet-interfaced high-resolution microendoscope with automated image interpretation for real-time evaluation of esophageal squamous cell neoplasia,” Gastrointest Endosc, 84 (5), 834 –841 (2016). https://doi.org/10.1016/j.gie.2016.03.1472

[28] D. Shin, M. A. Protano, A. D. Polydorides et al., “Quantitative analysis of high-resolution microendoscopic images for diagnosis of esophageal squamous cell carcinoma,” Clin Gastroenterol Hepatol, 13 (2), 272 –279 (2015). https://doi.org/10.1016/j.cgh.2014.07.030